STEM CELLS AND DEVELOPMENT
Volume 22, Number 19, 2013

DOI: 10.1089/scd.2013.0125

Epigenetic Regulation of the Electrophysiological Phenotype of Human Embryonic Stem Cell-Derived Ventricular Cardiomyocytes: Insights for Driven Maturation and Hypertrophic Growth

Maggie Zi Ying Chow,[1,2] Lin Geng,[2] Chi-Wing Kong,[1,2] Wendy Keung,[1,2] Jacky Chun-Kit Fung,[2] Kenneth R. Boheler,[1,3] and Ronald A. Li[1,2,4]

Epigenetic regulation is implicated in embryonic development and the control of gene expression in a cell-specific manner. However, little is known about the role of histone methylation changes on human cardiac differentiation and maturation. Using human embryonic stem cells (hESCs) and their derived ventricular (**V**) cardiomyocytes (CMs) as a model, we examined trimethylation of histone H3 lysine 4 (H3K4me3) and lysine 27 (H3K27me3) on promoters of genes associated with cardiac electrophysiology, contraction, and Ca^{2+} handling. To avoid ambiguities due to heterogeneous chamber-specific types, hESC-derived ventricular cardiomyocytes (**V**CMs) were selected by dual zeocin-GFP expression under the transcriptional control of the *MLC2v* promoter and confirmed electrophysiologically by its signature action potential phenotype. High levels of H3K4me3 are present on pluripotency genes in hESCs with an absence of H3K27me3. Human ESC-**V**CMS, relative to hESCs, were characterized by a profound loss of H3K27me3 and an enrichment of H3K4me3 marks on cardiac-specific genes, including *MYH6*, *MYH7*, *MYL2*, *cTNT*, and *ANF*. Gene transcripts encoding key voltage-gated ion channels and Ca^{2+}-handling proteins in hESC-**V**CMs were significantly increased, which could be attributed to a distinct pattern of differential H3K4me3 and H3K27me3 profiles. Treatment of hESC-**V**CMs with the histone deacetylase inhibitor valproic acid increased H3K4me3 on gene promoters, induced hypertrophic growth (as gauged by cell volume and capacitance), and augmented cardiac gene expression, but it did not affect electrophysiological properties of these cells. Hence, cardiac differentiation of hESCs involves a dynamic shift in histone methylation, which differentially affects **V**CM gene expression and function. We conclude that the epigenetic state of hESC-**V**CMs is dynamic and primed to promote growth and developmental maturation, but that proper environmental stimuli with chromatin remodeling will be required to synergistically trigger global CM maturation to a more adult-like phenotype.

Introduction

Human embryonic stem cells (hESCs) are pluripotent cells that can indefinitely propagate in culture and differentiate into virtually any cell type [1]. Since adult cardiomyocytes (CMs) are terminally differentiated and non-regenerative, significant loss of functional CMs due to aging or myocardial infarction can lead to lethal consequences. Using in vitro differentiation methods, ventricular (**V**) CMs derived from hESCs are considered as a valuable source for potential cell-based heart therapies and as experimental models for human heart diseases [2–6]. Previous studies have examined various biological properties of hESC-derived ventricular cardiomyocytes (**V**CMs), including ion channel development, action potential (AP), Ca^{2+} transients, and propagation of electrical signals [7–10]. Despite the expression of cardiac-specific transcription factors and structural proteins in the hESC-**V**CMs, it is now widely accepted that both the Ca^{2+} handling and electrophysiological properties of hESC-**V**CMs are immature (reviewed in [11]) with an underlying basis that is very poorly understood. Furthermore, hESC-**V**CMs are typically 5 to 10 times physically smaller than adult **V**CMs, and can generate contractile forces that are only a fraction of the adult level.

Chromatin modifications and epigenetic changes are central to the regulation of gene expression [12,13]. In particular,

[1]Stem Cell and Regenerative Medicine Consortium, The University of Hong Kong, Pok Fu Lam, Hong Kong.
[2]Department of Physiology, The University of Hong Kong, Pok Fu Lam, Hong Kong.
[3]Laboratory of Cardiovascular Science, National Institute on Aging, National Institutes of Health, Baltimore, Maryland.
[4]Center of Cardiovascular Research, Icahn School of Medicine at Mount Sinai, New York, New York.

histone modifications, including acetylation, methylation, phosphorylation, and ubiquitination, have received considerable attention in recent years [14–18]. Different histone modification patterns form histone codes, providing specialized binding surfaces that recruit protein complexes containing chromatin remodeling and transcriptional activation or repression activities [19,20]. Recent studies at the genome-wide level have identified important chromatin patterns of the embryonic epigenetic landscape. During the course of development, a balance between active (H3K4me3-enriched) and silent (H3K27me3-enriched) transcription is maintained by specific histone methyltransferases [21]. The repression of tissue-specific and developmental genes in pluripotent ESC is temporary and dynamic, and is based on the presence of bivalent chromatin domains, which are composed of active (H3K4me3) and repressive marks (H3K27me3), allowing them to become rapidly activated when required at a later stage of development [22–25].

With the key objective of understanding the epigenetic regulation in hESC-**V**CMs, in this report, using chromatin immunoprecipitation (ChIP) assays, patch-clamp and Ca^{2+}-imaging techniques, we examined the histone methylation status of hESC-**V**CMs on genes that are known to associate with pluripotency, cardiac functions, Ca^{2+} handling, and crucial ion channels. Collectively, our findings present that dynamic changes in epigenetic landscape in the context of histone methylation-mediated transcriptional regulation underlie human CM development and function.

Materials and Methods

Maintenance and cardiac differentiation of HES2

The hESC line, HES2, was maintained in 37°C with a 5% CO_2 incubator in an mTeSR®1 culture medium (Stem Cell Technologies). A directed differentiation protocol was used to differentiate HES2 into cardiac lineage using the activin A, bone morphogenetic protein-4 (BMP-4), and vascular endothelial growth factor (VEGF) induction, as reported [26]. In brief, on Day 0, HES2 were cultured in suspension to form cardiosphere aggregates using BMP4 (0.5 ng/mL). Day 1–4, the aggregates were incubated in media containing BMP4 (5 ng/mL), basic fibroblast growth factor (bFGF) (5 ng/mL), and activin A (3 ng/mL). Day 4–8, activin A and BMP4 were removed, and replenished with VEGF (10 ng/mL) and human Dickkopf homolog 1 (150 ng/mL). After Day 8, the cardiospheres were maintained in VEGF (10 ng/mL) and bFGF (5 ng/mL). The differentiation cultures were maintained in 5% CO_2/5% O_2/90% N_2 environment for the first 12 days, and then transferred into a normal 5% CO_2 incubator. Fresh media is supplied every 3 to 4 days.

Isolation and selection of hESC-VCMs

HESC-derived CMs are heterogeneous, containing a mixture of ventricular, atrial, and pacemaker derivatives [7,8]. To eliminate noncardiac cells and purify hESC-**V**CMs, cardiospheres were dissociated and replated as single cells on Day 17, and transduced with recombinant lentivirus particle, LV-MLC2v-GFP-t2A-zeo at MOI of 5 on Day 18. Zeocin™ (300 μg/mL) (Life Technologies) was added to the transduced cells from Day 22 to Day 27 to eliminate non-ventricular CMs. The effectiveness using MLC2v-promoter lentivirus for ventricular CM selection has been reported previously [27,28].

Histone deacetylase complex inhibition

Zeocin selected hESC-**V**CMs were exposed to valproic acid (VPA) (Sigma Chemical Co., Ltd.) at 2 mM for 48 h. VPA was prepared in the Dulbecco's modified Eagle medium culture medium containing 5% fetal bovine serum.

cDNA synthesis and gene expression analysis by real-time PCR

cDNA were prepared using the SuperScript® CellsDirect cDNA Synthesis Kit (Life Technologies) following the protocol recommended by the manufacturer. Gene expressions were quantified using StepOnePlus™ Real-Time PCR system (Applied Biosystems). PCR amplifications were carried out in 96-well optical plates with 20 μL reaction volume, consisting of 100 ng of cDNA template, 5 pmol of forward and reverse primers, and 1×Power SYBR® Green PCR Master Mix (Applied Biosystems). The reactions were incubated at 95°C for 10 min, and followed by 40 to 50 cycles of 95°C for 15 s and 60°C for 60 s. Primer sequences are available upon request.

ChIP assay

The ChIP assay was carried out using the EZ Magna ChIP™ A/G Kit (Millipore) following the protocol recommended by the manufacturer. In brief, isolated cells (5×10^6 cells) were crosslinked in a 1% formaldehyde solution, and then quenched by the addition of 0.125 M glycine. The crosslinked cells were then resuspended in a sodium dodecyl sulfate (SDS) lysis buffer, and the soluble chromatin was sheared to 200–500 bp in length by sonication. Protein A/G magnetic beads and 5 μg of antibodies (H3K4me3–Millipore 07-473 or H3K27me3–Millipore 07-449) were added to the fragmented chromatin and incubated for 2 h at 4°C with rotation. The immunocomplexes were collected by a magnetic separator, washed, and DNA was eluted with 1% SDS and 0.1 M $NaHCO_3$. DNA was purified using spin columns, and enrichment of specific histone modifications on gene promoters were quantified by real-time PCR as described above. Control ChIPs were also carried out to test antibody specificity using either no antibody or normal IgG. Primer sequences are available upon request.

Electrophysiology

For electrical recording, the whole-cell configuration of the patch-clamp technique was used with an EPC-10 amplifier and Pulse software (Heka Elektronik). Patch pipettes were prepared from 1.5-mm thin-walled borosilicate glass tubes using a Sutter micropipette puller P-97 and had typical resistances of 3-5 MΩ when filled with an internal solution containing 110 mM K^+ aspartate, 20 mM KCl, 1 mM $MgCl_2$, 0.1 mM Na-GTP, 5 mM Mg-ATP, 5 mM Na_2-phospocreatine, 1 mM EGTA, 10 mM HEPES, pH adjusted to 7.3 with KOH. The external Tyrode's bath solution consisted of 140 mM NaCl, 5 mM KCl, 1 mM $CaCl_2$, 1 mM $MgCl_2$, 10 mM glucose, 10 mM HEPES, pH adjusted to 7.4 with NaOH. The tip potential was zeroed before the patch pipette contacted the cell.

Upon seal formation and followed by patch break, the capacitance compensation was applied. Series resistance compensation was used up to 80%. APs were recorded with the current-clamp mode. Experiments were performed at 37°C.

Calcium imaging

The intracellular Ca^{2+} ($[Ca^{2+}]_i$) transients were analyzed by loading the cells with 1.5 μM X-Rhod-1 (Invitrogen) for 10 min at 37°C in the Tyrode's solution containing 140 mM NaCl, 5 mM KCl, 1 mM $MgCl_2$, 1.25 mM $CaCl_2$, 10 mM HEPES and 10 D-glucose at pH 7.4), followed by imaging with a spinning disc laser confocal microscope (PerkinElmer). The electrically induced Ca^{2+} transients ($E[Ca^{2+}]_i$) were triggered by pulses (40 ms pulse duration; 40 V/cm; 1 Hz) generated from a field generator. The amplitudes of Ca^{2+} transients are presented as the background corrected pseudoratio $(\Delta F/F)^{1,2} = (F\text{-}F_{base})/(F_{base}\text{-}B)$, where F_{base} and F is the measured fluorescence intensity before and after stimulation, respectively, and B is the average background signal from areas adjacent to the targeted cell. The transients rise ($V_{upstroke}$) and the transients decay (V_{decay}) were subsequently calculated and analyzed.

Cell volume

The cell volume of hESC-**V**CMs was determined by immunostaining the fluorescent dye CellTracker™ Green (Invitrogen). A z-stack image was then obtained with a confocal microscope (Carl Zeiss LSM 510 meta). The 3D image was constructed and cell volume was estimated with the image analysis software Imaris.

Immunofluorescence imaging

hESC-**V**CMs were fixed with 4% paraformaldehyde and permeabilized with 0.05% Triton X-100. After blocking with 3% bovine serum albumin overnight, cells were incubated with the primary antibody for 2 h (Sarcomeric alpha actinin [EA-53]–Abcam ab9465; Cardiac troponin T [1F11]–Abcam ab10214; Myosin light chain 2–Abcam ab79935; SERCA2 ATPase [2A7-A1]–Abcam ab2861, atrial natriuretic peptide (ANP)–Abcam ab76743) followed by incubation with fluorescent-conjugated secondary antibodies (Alexa Fluor 488 or 555–Life Technologies). Fluorescence images were captured and analyzed using Spot Advance software (Spot™ Imaging Solutions). The percentage of ANP natriuretic peptide type A (NPPA)-positive cells was calculated by counting the number of cells with a strong perinuclear fluorescence signal around the nucleus stained by DAPI (ProLong® Gold Antiface Reagent with DAPI–Molecular Probes®).

Results

Zeocin-selected GFP-positive LV-MLC2v-GFP-t2A-zeo-transduced hESC-CMs displayed a ventricular phenotype

As reported previously, the expression of a reporter protein driven by the ventricular myosin light chain (MLC2v) promoter enables the identification and isolation of hESC-**V**CMs [27,28]. In these experiments, LV-MLC2v-GFP-t2A-zeo transduction was performed, followed by zeocin selection. Figure 1A, B shows a typical pure population of zeocin-selected GFP^+ cells that were positively immunostained for cTNT, MLC2v, α-sacromeric actinin, and SERCA2a. Electrophysiologically, all of the GFP^+ cells ($n = 30$) displayed an AP waveform (Fig. 1C) as well as electrically elicited Ca^{2+} transients (Fig. 1D) that were typical of hESC-**V**CMs. Throughout this study, only selected hESC-**V**CMs were examined to avoid ambiguities due to the presence of other chamber-specific types.

Distinct gene expression profiles of hESCs and hESC-VCMs

As a first step, we compared the differential intensity obtained from microarray profiling [28] of undifferentiated hESCs and hESC-**V**CMs. Supplementary Figure S1(Supplementary Data are available online at www.liebertpub.com/scd) shows a unique pattern of increased abundances for cardiac-specific genes, Ca^{2+}-handling proteins, and various cardiac ion channels in hESC-**V**CMs compared to hESCs; conversely, signal intensities of pluripotency markers, including *OCT4*, *SOX2*, and *NANOG*, were significantly reduced in hESC-**V**CMs. To validate this trend, the expression levels of several representative pluripotency and cardiac genes in hESCs and hESC-**V**CMs were further assessed using quantitative real-time PCR. As shown in Fig. 2A, hESC-**V**CMs expressed markers of mesodermal lineage commitment, *MESP1*, and cardiac progenitor, *ISL1*. There was also a significant increase in the expression of the cardiac transcription factor *Nkx2.5* as well as the cardiac-specific genes *cTNT* and *MLC2v*. By contrast, transcripts of pluripotency, including *OCT4* and *NANOG*, were significantly expressed in hESCs, but not hESC-**V**CMs (Fig. 2B). As for Ca^{2+}-handling proteins (Fig. 2C), phospholamban (*PLN*), dihydropyridine receptor (*DHPR*), ryanodine receptor 2 (*RYR2*), junction (*ASPH/JCTN*), ATPase calcium transporting cardiac muscle slow twitch 2 (*ATP2A2/SERCA2*), calreticulin (*CALR*), calsequestrin2 (*CASQ2*), and triadin (*TRDN*) all showed a significant increase in their expression levels in hESC-**V**CMs compared to hESCs. Of note, mRNA transcripts of *PLN* and *CASQ2* were below detectable levels in undifferentiated hESCs. Similarly, examination of voltage-gated sodium channel—*SCN5A* ($Na_v1.5$)—hyperpolarization-activated cyclic nucleotide-gated potassium channel—*HCN1*, *HCN2*, and *HCN4*—and voltage-gated potassium channels—*KCNA4* ($K_v1.4$), *KCND3* ($K_v4.3$), *KCNH2* (*ERG1*), and *KCNJ2* (*Kir2.1*)—were all upregulated in the hESC-**V**CMs. No significant difference was detected for *HCN3*, as the levels of mRNA transcripts were low in both hESCs and hESC-**V**CMs. Summary of the gene expression analyses is shown in Supplementary Table S1.

Differential enrichment of H3K4tri-methylation and H3K27tri-methylation on gene promoters

The presence of specific methylation marks on gene promoters has been associated with transcriptional regulation. Using ChIP, the levels of H3K4 tri-methylation (H3K4me3—associated with active transcription) and H3K27 tri-methylation (H3K27me3—associated with repressed transcription) on gene promoters (< 1000 bp from transcriptional initiation site) were compared between hESCs and hESC-**V**CMs. On promoters of pluripotency genes, *OCT4*, *SOX2*, and *NANOG*, there was an accumulation of H3K4me3 in hESCs (Fig. 3A),

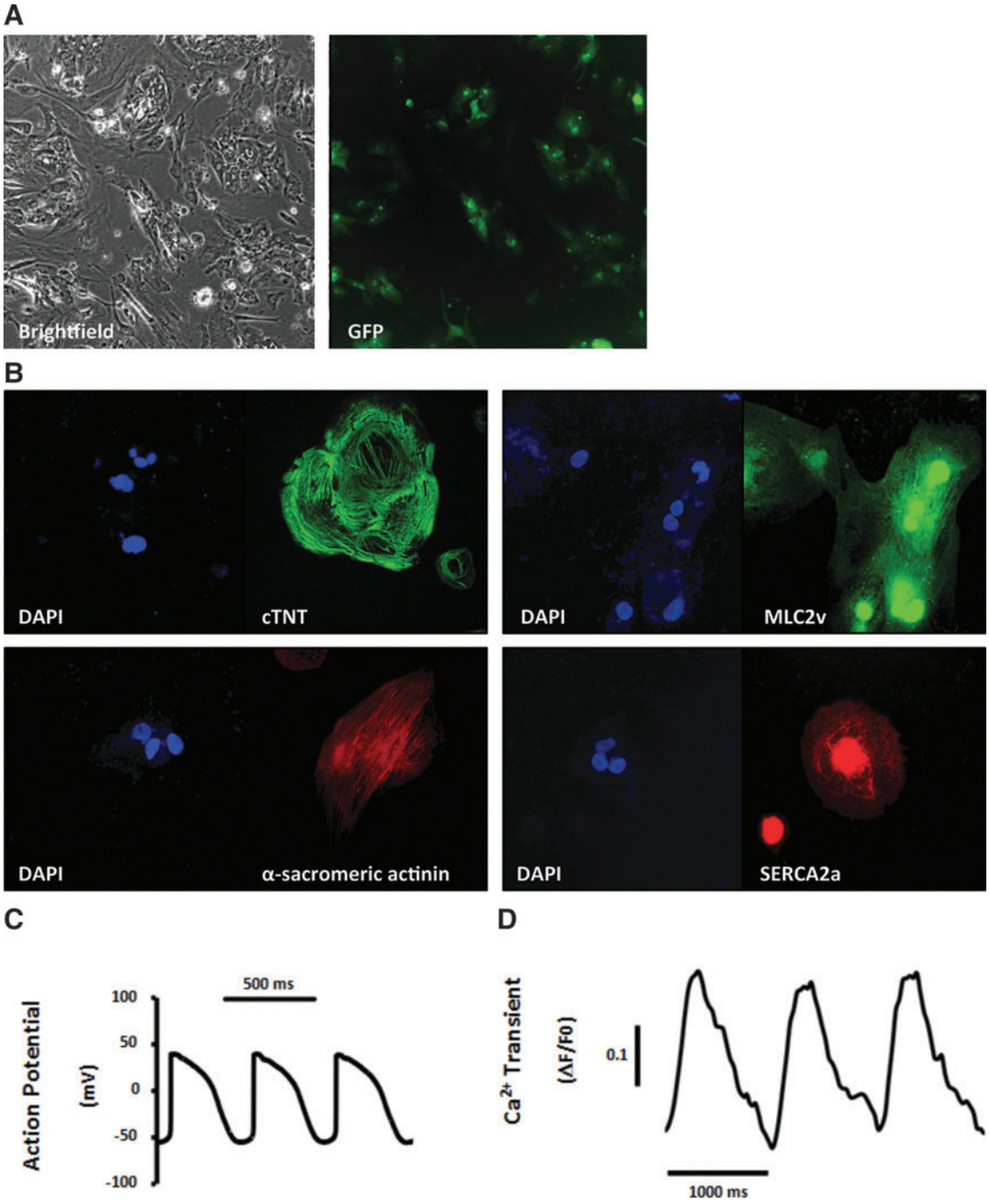

FIG. 1. Characterization of zeocin selected MLC2v-GFP-positive human embryonic stem cell-derived ventricular cardiomyocytes (hESC-**V**CMs). **(A)** Brightfield (*left panel*) and fluorescence (*right panel*) imaging of LV-MLC2v-GFP-t2A-zeo-transduced hESC-CMs after 7 days of zeocin selection. Images were captured at 10×magnification. **(B)** Immunofluorescence staining of cTnT, MLC2v, α-sacromeric actinin, and SERCA2a of hESC-**V**CMs. Images were captured at 40×magnification. **(C)** Representative tracing of action potential (AP) and **(D)** electrically induced Ca^{2+} transient in hESC-**V**CMs at 1 Hz. Color images available online at www.liebertpub.com/scd

whereas H3K27me3 was enriched on these regions in hESC-**V**CMs (Fig. 4A). Conversely, H3K27me3 was significantly higher on cardiac genes in hESCs (Fig. 4B), but H3K4me3 was enriched on the *MLC2v*, *MLC2a*, *cTNT*, and *NPPA* promoters in hESC-**V**CMs (Fig. 3B). These results correlated with the gene expression data. The interplay between H3K4me3 and H3K27me3 were similarly studied on the cardiac ion channel and Ca^{2+}-handling genes. While there was a significant increase in H3K4me3 on the *PLN*, *DHPR*, *ASPH*, *TRDN*, *SCN5A*, and *KCNA4* promoters in hESC-**V**CMs when compared to hESCs (Fig. 3C, D), reduction in H3K27me3 is observed on *PLN*, *CALR*, *CASQ2*, and *TRDN* promoters (Fig. 4C). No statistical differences were detected for H3K27me3 and H3K4me3 on the promoters of other cardiac ion channels and proteins examined (e.g., *RYR2*, *SERCA2*, *HCN1-4*, *KCND3*, *KCNH2*, *and KCNJ2;* Figs. 3 & 4).

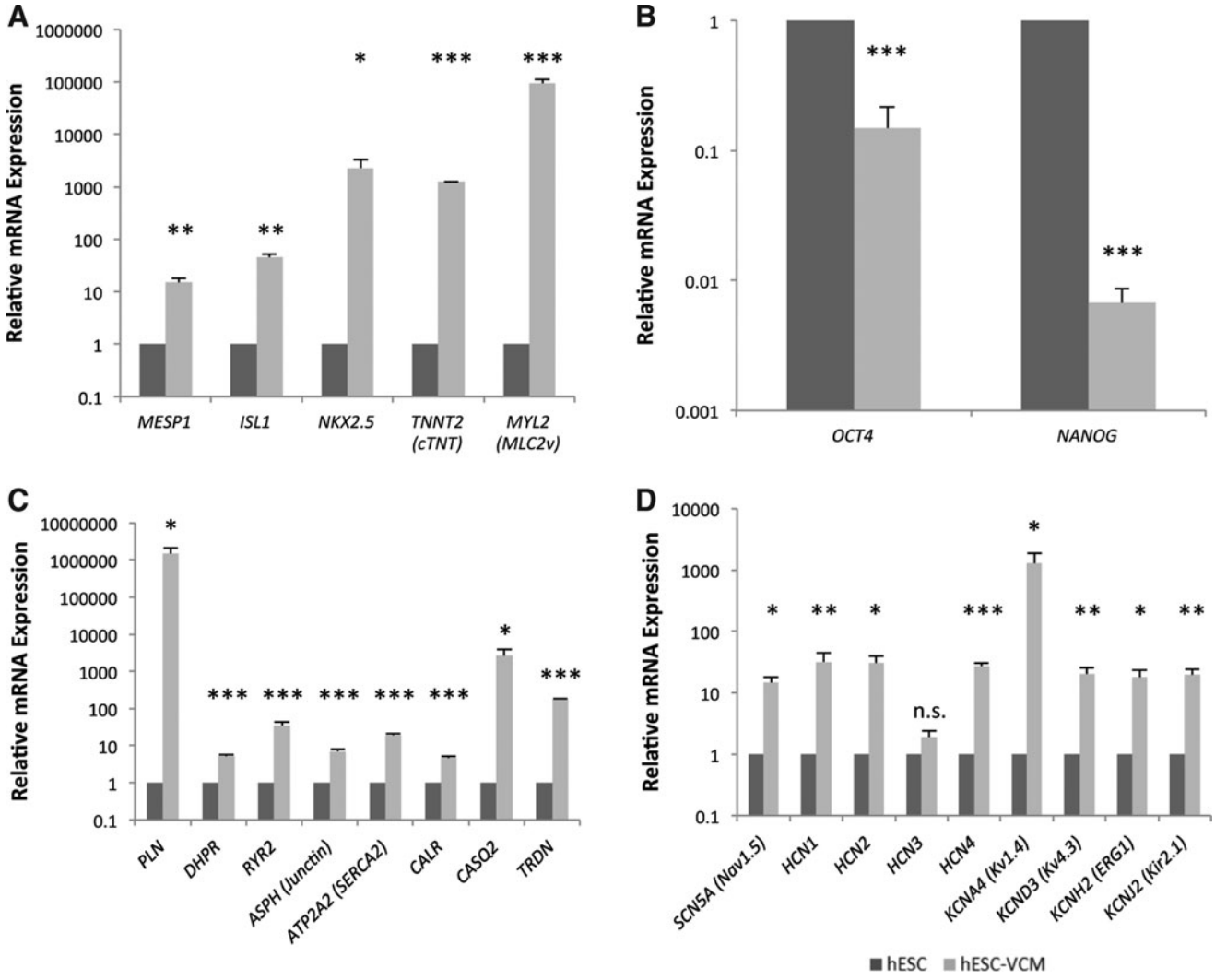

FIG. 2. Quantitative real-time PCR analysis of gene expression in hESCs and hESC-**V**CMs. The levels of mRNA transcripts of **(A)** cardiac-related genes [*MESP1*, *ISL1*, *NKX2.5*, (*TNNT*) *cTNT*, and *MYL2* (*MLC2v*)], **(B)** pluripotency markers (*OCT4* and *NANOG*), **(C)** Ca^{2+}-handling proteins (*PLN*, *DHPR*, *RYR2*, *ASPH*, *ATP2A2*, *CALR*, *CASQ2*, and *TRDN*), and **(D)** sodium and potassium ion channels [*SCN5A* (*Nav1.5*), *HCN1-4*, *KCNA4* ($K_v1.4$), *KCND3* ($K_v4.3$), *KCNH2* (*ERG1*), and *KCNJ2* (*Kir2.1*)] in hESCs and hESC-**V**CMs were compared using quantitative real-time PCR. Fold change of mRNA expression shown are relative to hESCs, and mean ± standard deviations of three independent experiments are indicated. $^*P < 0.05$, $^{**}P < 0.01$, $^{***}P < 0.001$ and n.s., not statistically significant (Student's *t*-test).

Histone deacetylase complex inhibition induced physical maturation in hESC-VCMs without altering their electrophysiological and Ca^{2+}-handling properties

Histone deacetylase (HDAC) inhibitors have often been used to hyperacetylate histone tails to increase the accessibility for the binding of transcription factors to promoters for gene activation. VPA (2-propylpentanoic acid) is structurally similar to the well-known HDAC inhibitors, such as sodium butyrate and phenylbutyrate, but it is less potent in terms of inhibition of HDAC than the hydroxymate class, which includes Trichostatin A (TSA) and suberoylanilide hydroxamic acid [29]. Western blotting analysis indicated that 72-h incubation of hESC with 2 mM VPA resulted in the accumulation of hyperacetylated histone H3 and H4 (Fig. 5A). Furthermore, the active transcription mark, H3K4me3, was enhanced upon VPA treatment. To examine the effect of HDAC inhibition on hESC-**V**CMs, cells were likewise exposed to 2 mM VPA for 72 h, followed by examining any transcription changes by quantitative real-time PCR. There was 1.5- to 3.5-fold increase in the expression of genes associated with Ca^{2+} pump and K^+ ion channels (Fig. 5B, C) in the VPA-treated hESC-**V**CMs. The expression of cardiac markers, *MYH6* (*α-MHC*), and hypertrophy markers, *NPPA* (*ANF*), also increased by 1.9- and 1.6-fold, respectively (Fig. 5D). Immunofluorescence imaging showed the accumulation of NPPA in the hESC-**V**CMs at 72 h following VPA treatment (Fig. 5E). By counting and measuring the percentage of cell with the perinuclear atrial natriuretic factor (ANF), it is found that 31% of the control hESC-**V**CMs and 51% of the VPA-treated hESC-**V**CMs were ANF-positive (Fig. 5F). In addition to the global increase of H3K4me3 upon VPA treatment, immunoprecipitation of H3K4me3-bounded DNA indicated that there was an

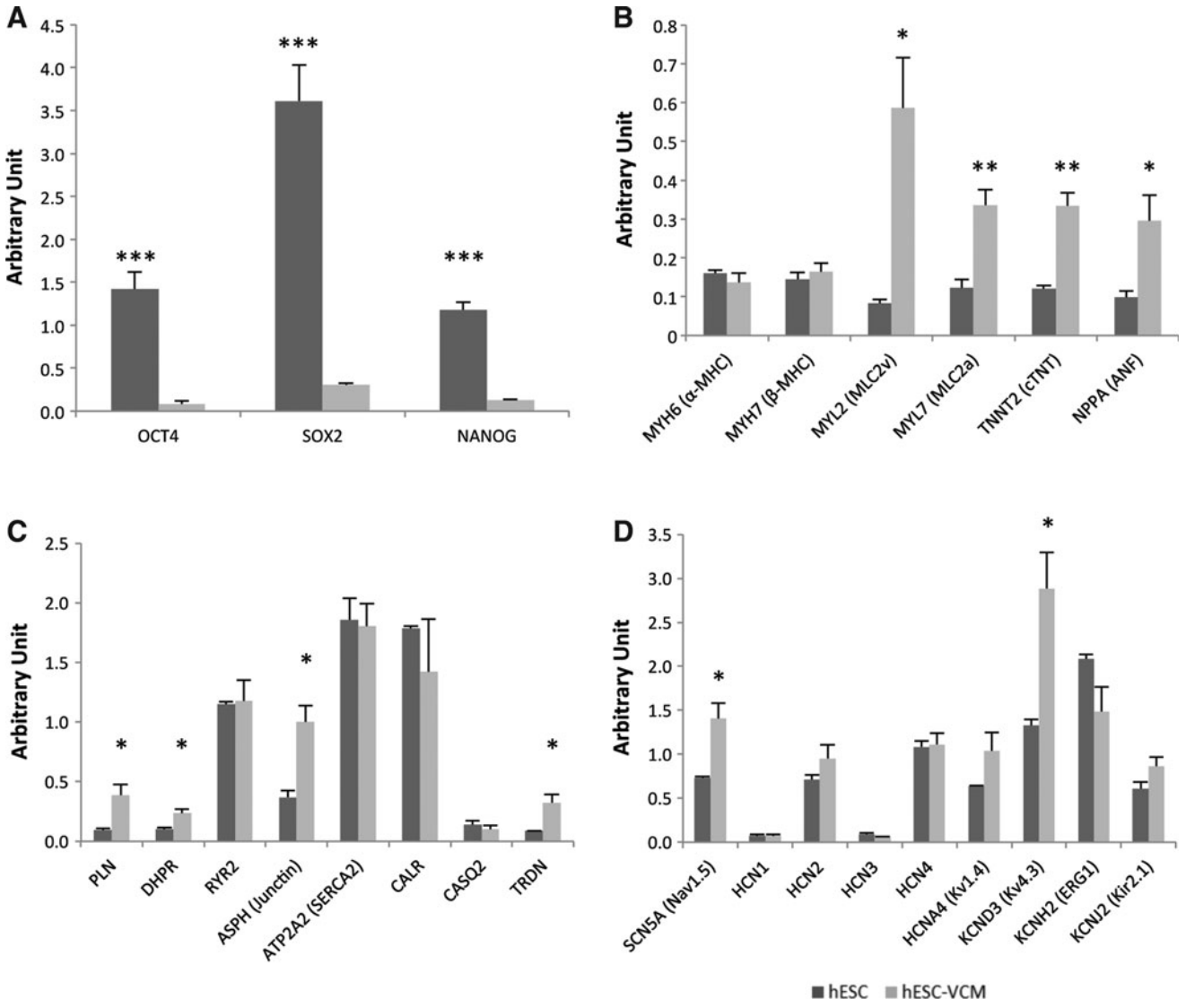

FIG. 3. The levels of H3K4tri-methylation on gene promoters in hESCs and hESC-**V**CMs. Soluble chromatin of hESCs and hESC-**V**CMs were immunopurified using the H3K4me3 antibody and quantitative real-time PCR was used to measure the level of enrichment on gene promoters associated with **(A)** pluripotency, **(B)** cardiac-related genes, **(C)** Ca^{2+}-handling proteins, and **(D)** sodium and potassium ion channels. Data were normalized to input chromatin and relative to the level of enrichment on the *GAPDH* promoter (transcriptionally active). Mean ± standard deviations of three independent experiments are presented. $^{*}P < 0.05$, $^{**}P < 0.01$, and $^{***}P < 0.001$ (Student's *t*-test).

enrichment of this active transcription mark at the chromatin level, by 3- to 10-fold, on the gene promoters of Ca^{2+}-pump functions and ion channels (Fig. 5G). Of interest, the level of H3K4me3 on the *NPPA* promoter was 91-fold higher in the hESC-**V**CMs after VPA treatment.

Despite increased gene expression of Ca^{2+}-handling proteins and ion channels, hyperacetylation of histone tails by VPA did not lead to significant electrophysiological changes of hESC-**V**CMs. The percentages of hESC-**V**CMs that could be captured by electrical stimulations were similar between hESC-**V**CMs with or without exposure to VPA ($P > 0.05$). There were also no significant differences in the baseline Ca^{2+}-transient amplitude, upstroke velocity, and decay velocity between the untreated controls (noncaptured $n = 43$; captured $n = 12$) and the hESC-**V**CMs incubated with 2 mM of VPA for 72 h (noncaptured $n = 25$; captured $n = 20$) (Table 1). Representative Ca^{2+}-transient traces are shown in Fig. 6A. HESC-**V**CMs were also examined for their responsiveness to β-adrenergic stimulation. Among the hESC-**V**CMs that captured electrical stimulation, β-agonist isoproterenol (ISO) led to a positive chronotropic response, but failed to elicit any inotrophic effects on cells as no significant difference in Ca^{2+}-transient parameters was detected (untreated $n = 7$; VPA-treated $n = 12$) (Table 1), consistent with untreated control. In the AP analysis by patch clamp, the electrical properties of the control ($n = 25$) and VPA-treated ($n = 23$) hESC-**V**CMs were similar with no statistical significance (Fig. 6B), but VPA treatment promoted cell enlargement as indicated by the significant increase in membrane capacitance (Fig. 6C, Table 2). In complete accordance with these observations, hESC-**V**CMs immunostained by CellTracker™ Green for cell volume measurement were

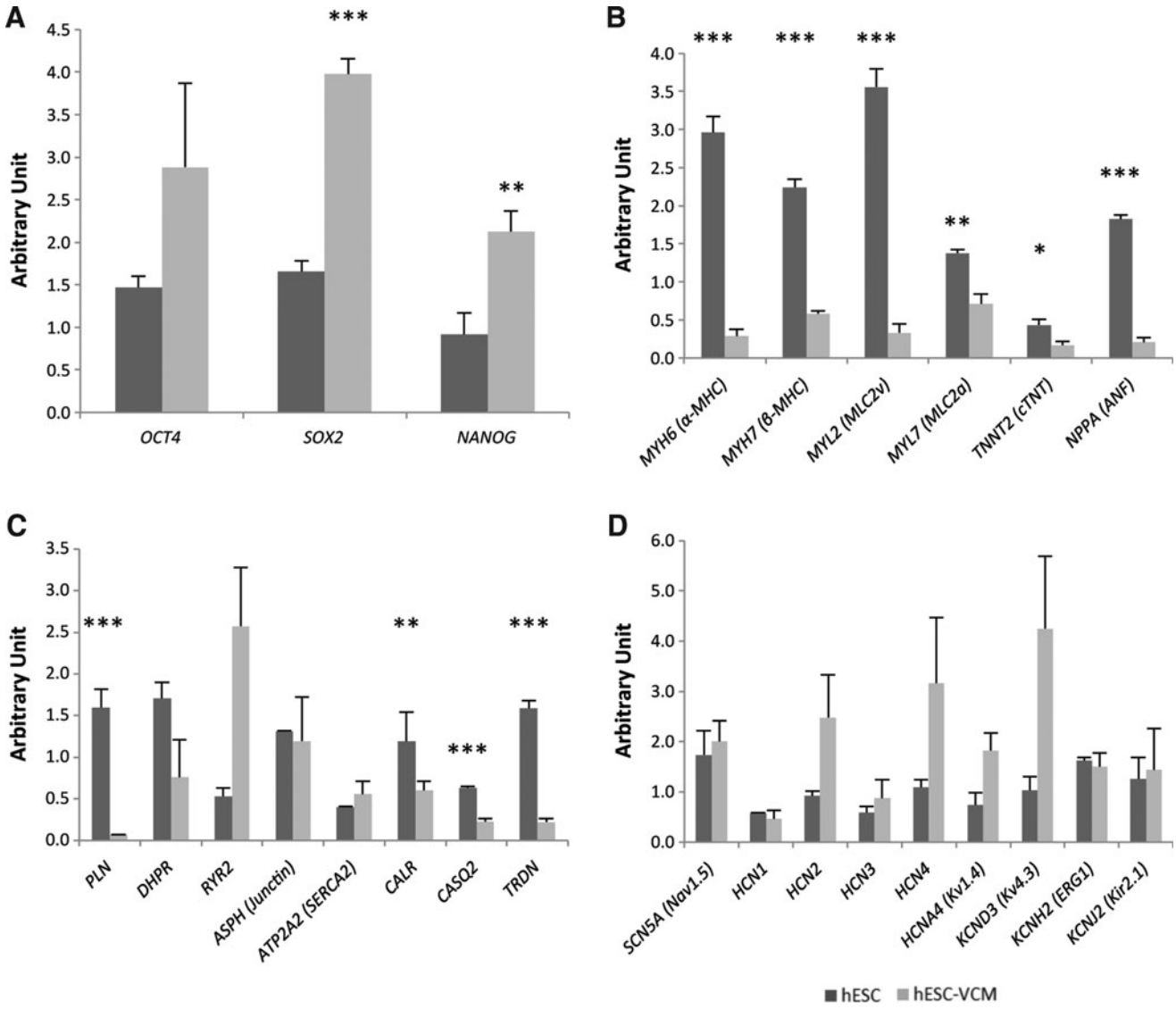

FIG. 4. The levels of H3K27tri-methylation on gene promoters in hESCs and hESC-**V**CMs. Soluble chromatin of hESCs and hESC-**V**CMs were immunopurified using the H3K27me3 antibody and quantitative real-time PCR was used to measure the level of enrichment on genes associated with **(A)** pluripotency, **(B)** cardiac-related genes, **(C)** Ca^{2+}-handling proteins, and **(D)** sodium and potassium ion channels. Data were normalized to input chromatin and relative to the level of enrichment on the Satelite1 region (transcriptionally silenced). Mean ± standard deviations of three independent experiments are presented. $^{*}P < 0.05$, $^{**}P < 0.01$, and $^{***}P < 0.001$ (Student's *t*-test).

almost three times larger in VPA-treated hESC-**V**CMs ($n = 18$) than untreated controls ($n = 18$) (Fig. 6D).

Discussion

Characterization of the histone methylation profile and transcriptional regulation of genes encoding for Ca^{2+}-handling proteins and cardiac ion channels in this study provide molecular insights of the epigenetic mechanism associated with the electrophysiology functions of hESC-**V**CMs. In particular, we showed that upon cardiac differentiation, the upregulation of cardiac-specific genes and downregulation of pluripotency maintenance genes are tightly correlated with H3K4me3 (active transcription mark) and H3K27me3 (silent transcription mark). Epigenetic manipulation with a HDAC inhibitor, VPA, increased the expression of genes associated with Ca^{2+}-handling proteins and cardiac ion channels, with the enrichment of active H3K4me3 marks on their corresponding gene promoters. Finally, we extended our study to investigate the effect of VPA treatment on the electrophysiology functional properties of CMs. In the process, we discovered that VPA treatment appears to induce developmental hypertrophic growth, as gauged by cell volume and membrane capacitance. These results are further discussed below in the context of driven maturation and mechanistic insights.

Distinct modes of histone modification regulations: hESC-VCMs are epigenetically primed for maturation, but need triggering environmental stimuli

Gene transcription is tightly regulated by three important epigenetic mechanisms, DNA methylation, post-translational

modifications of histones, and ATPase-dependent chromatin remodeling [30]. Chromatin determinants and transcription factors function together for genes to be selectively activated or silenced in response to chemical and environmental stimuli [31]. Previous studies have demonstrated that the H3K4-methylation complex is essential for stabilizing gene expression and physiological functions of CMs [32]. Also, the upregulation of *Nkx2.5* is accompanied by the increase of histone H3 and H4 acetylation and the reduction of HDAC1 expression [33]. The histone tails of *MYH6* is also targeted by histone acetyltransferases in CMs [34]. Using the hESC-**V**CMs generated by directed differentiation, we not only observed the fundamental changes in gene regulation, including the loss of pluripotency-related genes expression, accompanied by the high expression of mesodermal and cardiac-related genes, we also demonstrated the activation of important genes encoding for proteins that are responsible for the control of Ca^{2+} pumping and ion transports between the cytoplasm and sarcoplasmic reticulum lumen. In undifferentiated hESCs, the active *OCT4*, *SOX2*, and *NANOG* promoters are enriched by the active transcription mark—H3K4me3. Upon CM differentiation, H3K4me3 is lost on these pluripotency gene promoters and the enrichment of H3K27me3 is observed. Furthermore, for the establishment of CM development, dynamic changes of the persisting epigenetic marks occur to create a chromosomal environment that favors the upregulation of genes responsible for CM contraction, Ca^{2+} handling, and cardiac ion channels. Our results are consistent with recent next generation sequencing (ChIP-sequencing (SEQ) and RNA-SEQ) analyses, which provide insights for the underlying regulatory mechanism that controls developmental transition in the cardiac lineage [35,36]; specific chromatin regulatory patterns are shared among functionally related and coexpressed genes for precise coordination of CM differentiation and development in mouse and human ESC cardiac differentiation models [35,36]. Interesting findings from genome-wide ChIP-SEQ reveal that unlike early lineage-specific genes that possess bivalent domain on the promoters in undifferentiated state, different subsets of cardiac-related genes have distinct histone methylation landscapes and are not entirely regulated by bivalent methylation. While a complete reversal of active and silent histone marks is found on pluripotency-associated gene promoters, upon CM differentiation, genes involved in mesoderm formation are highly expressed despite being heavily marked by H3K27me3 [36]. Developmental regulators such as cardiac-specific transcription factors are highly enriched for H3K27me3 in the undifferentiated state, which gradually decrease as H3K4me3, H3K36me3, and mRNA expression appear. In contrast, genes encoding for CM contractile and structural proteins, do not have high levels of H3K27me3 deposition at any time [36]. These distinct modes of histone modification regulations have been suggested to exist to ensure that particular gene sets of specific functions can be switched on simultaneously. This is consistent with our postulation that the hESC-**V**CMs are primed to maturation, but need to be stimulated by the right signals or environmental stimuli. Indeed, we have reported that by mimicking endogenous fetal heart pacing by field stimulation in culture, the regulated rhythmic electrical conditioning of hESC-CMs promotes in vitro electrophysiological Ca^{2+} handling, as well as contractile maturation with more organized myofilaments [37].

Combinatorial approach for driving global maturation

An epigenetic drug that possesses a known inhibitory effect on HDACs was used in this study to modify the transcriptional regulation in hESC-**V**CMs. Use of HDAC inhibitors in ESC differentiation has been previously reported. For instance, TSA facilitates myocardial differentiation of the murine induced pluripotent stem cell [38] and increases acetylation of GATA-binding protein-4 to promote differentiation of murine ESCs into CMs [39]. VPA is a Food and Drug Administration approved drug that is clinically used as an anticonvulsant, and a mood stabilizing drug for the treatment of epilepsy and bipolar disorder [40]. Recently, VPA has been shown to increase histone acetylation of histone H3 and H4, as well as enhance mono-, di-, and trimethylation at H3K4 [41,42]. The addition of VPA in hESC-**V**CM culture augmented the expression of genes important for electrophysiological functions. While no significant difference in AP and Ca^{2+}-transient properties was observed, VPA application induces developmental hypertrophic growth, as gauged by cell volume and capacitance, of hESC-**V**CMs that are typically physically 5 to 10 times smaller than the adult. It is possible that in addition to building an epigenetic state that is appropriate for improving electrophysiological functions, a combinatorial approach of simultaneously introducing proper environmental stimuli can couple with chromatin remodeling to synergistically trigger global CM maturation.

To improve the immature electrophysiology, inefficient excitation–contraction coupling and weak contractile force in

FIG. 5. Valproic acid (VPA) increased mRNA expression of Ca^{2+}-handling proteins and ion channel genes, and induced hypertrophy of hESC-**V**CMs. **(A)** hESCs were treated with 2 mM of VPA or 50 ng/μL of Trichostatin A (TSA) for 72 h and protein extracts were resolved on sodium dodecyl sulfate–polyacrylamide gel electrophoresis and analyzed by western blotting with either acetyl-H3, acetyl-H4, or H3K4me3 antibodies. Total histone H4 and GAPDH were used to demonstrate equivalent protein loading. hESC-**V**CMs were treated with 2 mM of VPA for 72 h and mRNA expression of genes related to **(B)** Ca^{2+}-handling proteins, **(C)** ion channels, and **(D)** cardiac hypertrophy were measured by quantitative real-time PCR. Mean ± standard deviations of three independent experiments are presented. $^{*}P < 0.05$, $^{**}P < 0.01$ and, $^{***}P < 0.001$ (Student's *t*-test). **(E)** Immunofluorescence staining of α-sacromeric actinin (*green*) and NPPA (ANF) (*red*) in control and VPA-treated hESC-**V**CMs. The images were captured at 40× magnification. **(F)** Percentage of NPPA (ANF)-positive immunostained cell in control untreated and VPA-treated hESC-**V**CMs (results from three independent experiments). **(G)** Representative data of H3K4me3 chromatin immunoprecipitation. Soluble chromatin of control and VPA-treated hESC-**V**CMs were immunopurified using the H3K4me3 antibody and quantitative real-time PCR was used to measure the level of enrichment on gene promoters. Data were normalized to input chromatin and relative to the level of enrichment in control untreated hESC-**V**CMs. Color images available online at www.liebertpub.com/scd

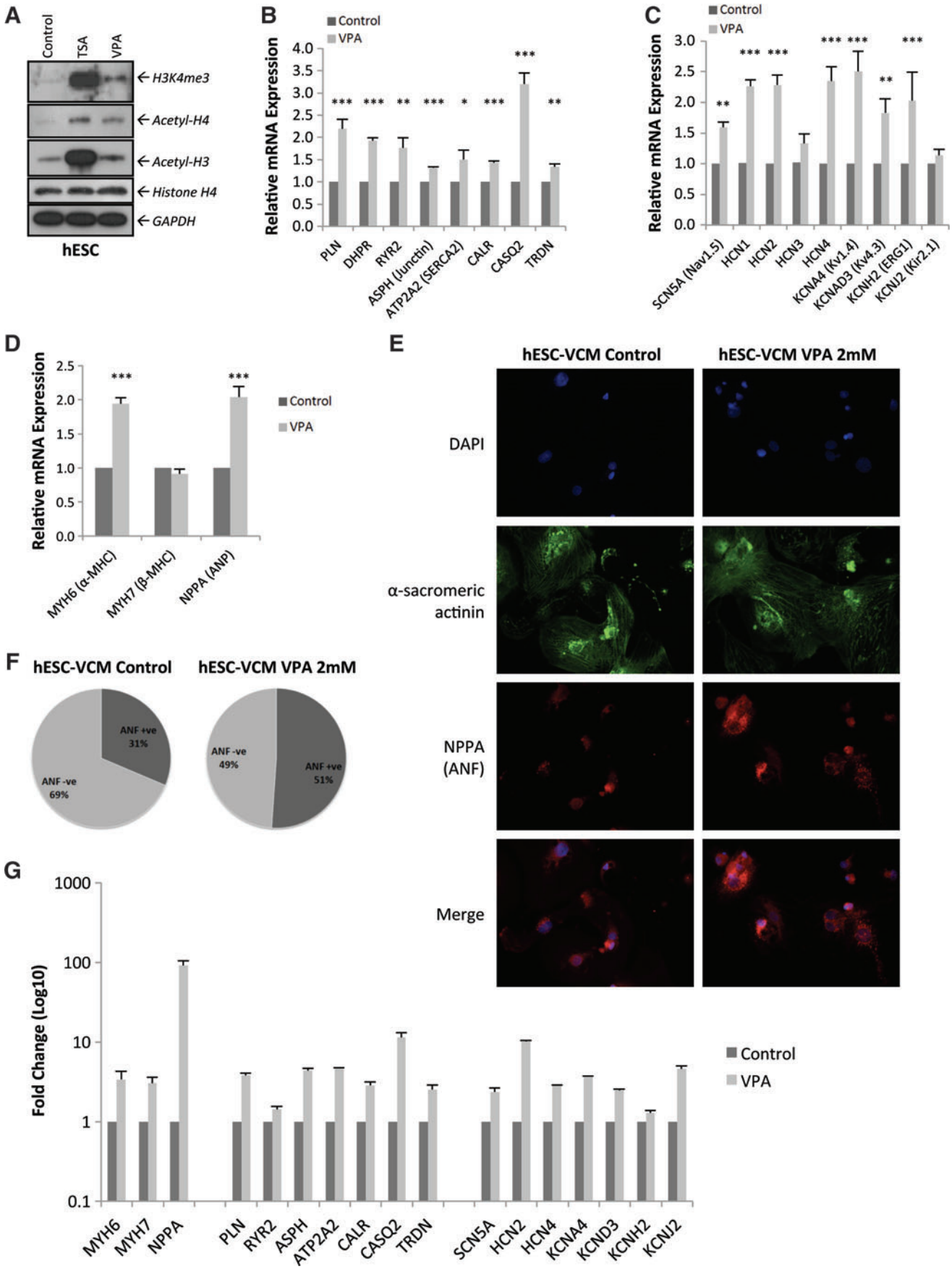
A
Control
TSA
VPA
H3K4me3
Acetyl-H4
Acetyl-H3
Histone H4
GAPDH
hESC
B
Control
VPA
Relative mRNA Expression
PLN
DHPR
RYR2
ASPH (Junctin)
ATP2A2 (SERCA2)
CALR
CASQ2
TRDN
C
Control
VPA
Relative mRNA Expression
SCN5A (Nav1.5)
HCN1
HCN2
HCN3
HCN4
KCNA4 (Kv1.4)
KCNAD3 (Kv4.3)
KCNH2 (ERG1)
KCNJ2 (Kir2.1)
D
Relative mRNA Expression
Control
VPA
MYH6 (α-MHC)
MYH7 (β-MHC)
NPPA (ANP)
E
hESC-VCM Control
hESC-VCM VPA 2mM
DAPI
α-sacromeric actinin
NPPA (ANF)
Merge
F
hESC-VCM Control
hESC-VCM VPA 2mM
ANF +ve 31%
ANF -ve 69%
ANF -ve 49%
ANF +ve 51%
G
Fold Change (Log10)
Control
VPA
MYH6
MYH7
NPPA
PLN
RYR2
ASPH
ATP2A2
CALR
CASQ2
TRDN
SCN5A
HCN2
HCN4
KCNA4
KCND3
KCNH2
KCNJ2

Table 1. Ca^{2+}-Transient Analysis (Calcium Imaging)

	Noncaptured		*Captured*	
	Control (n = 43)	*VPA (n = 25)*	*Control (n = 12)*	*VPA (n = 20)*
Amplitude	0.29 ± 0.03	0.27 ± 0.03	0.29 ± 0.05	0.24 ± 0.35
Upstroke velocity	0.89 ± 0.10	0.87 ± 0.10	1.27 ± 0.26	0.91 ± 0.16
Decay velocity	− 0.35 ± 0.03	− 0.45 ± 0.06	− 0.47 ± 0.12	− 0.34 ± 0.05
	Untreated hESC-VCM (n = 7)		*VPA-treated hESC-VCM (n = 13)*	
	Control	*Control + ISO*	*VPA*	*VPA + ISO*
Amplitude	0.37 ± 0.07	0.31 ± 0.05	0.23 ± 0.05	0.15 ± 0.04
Upstroke velocity	1.62 ± 0.35	1.39 ± 0.27	0.88 ± 0.24	0.64 ± 0.16
Decay velocity	− 0.62 ± 0.15	− 0.79 ± 0.17	− 0.35 ± 0.08	− 0.34 ± 0.07

hESC, human embryonic stem cell; VPA, valproic acid; ISO, isoproterenol.

hESC-**V**CMs, re-expression of the proteins important for these functions are essential. Indeed, microarray data suggest that the gene expression levels of *PLN*, *RYR2*, *ASPH*, *CASQ2*, *KCND3*, *KCNH2*, and *KCNJ2* in the hESC-**V**CMs are still lower than the mature CMs [28], and previous studies that examined the expression of key Ca^{2+}-handling proteins and ion channels at the protein level have reported that PLN, CASQ2, TRDN, and ASPH proteins are absent in the hESC-**V**CMs [32,43]. Our group has previously reported that facilitated maturation by forced expression of *CASQ2* can lead to functional improvements in Ca^{2+}-handling properties of hESC-**V**CMs [44], and overexpression of *Kir2.1* alone can even induce an electrical phenotype indistinguishable from that of primary adult ventricular cells [37,45,46]. Further investigation into manipulation of epigenetics, proteins, and physiological determinants, in combination, can potentially provide novel means to increase contractility and generate hESC-**V**CMs of a more mature state.

HDAC inhibition induces hypertrophic growth of hESC-VCMs, but their biological actions are context dependent

HDACs are grouped into four classes (I–IV). Class IIa HDACs interact with the transcription factor MEF2 to regulate cardiac hypertrophy. Overexpression of Class IIa HDACs 4, 5, and 9 suppresses MEF2-dependent transcription and agonist-dependent hypertrophy of cultured CMs [34,47,48]. In contrast, HDAC5 and HDAC9 knockout mice develop hypertrophy with increased age and show an exaggerated hypertrophic response to pressure overload [34,49]. On the other hand, Class I HDACs (1 and 2) are reported to promote hypertrophy. Cardiac-specific overexpression of HDAC2 in the transgenic mice model develops cardiac hypertrophy with increased fetal gene expression. Recent studies have demonstrated that Class IIa HDACs are actually relatively insensitive to standard HDAC inhibitors and do not require the catalytic activity to suppress hypertrophic signaling in CMs [50]. This is why HDAC inhibitors, via inactivation of Class I HDACs, generally cause attenuation in hypertrophy [51–54]. However, it should be noted that the majority of the studies were performed on murine models and hESC-**V**CMs used in our study actually represent an early stage of CM development, resembling immature fetal-like CMs. While the myosin composition of the ventricular myocardium of a human has been reported to be > 95% β-MHC, from examination of myosin gene expression during CM differentiation, genome-wide microarray, and proteomics analysis (Supplementary Figs. S1A and S2), α-MHC seems to be the predominant myosin isoform in hESC-**V**CMs. In addition to immature electrophysiology and contractile properties in the hESC-**V**CMs, their physical size is typically 5 to 10 times smaller than adult **V**CMs. CMs lose the ability to divide after birth and the adult heart undergoes cardiac hypertrophy in response to exercise, hormonal stimuli, and even genetic influences [55]. Although expression of ANF is a marker of both physiological and pathological hypertrophy in adult ventricular CMs, in the case of immature fetal ventricular CMs, the expression of ANF is most consistent with the development of a working myocardium [56].

From whole genome analysis, the expression profiles of CMs at different developmental stages vary. Our group has previously demonstrated that miR-1 and −499 have differential effects in hESC-**V**CMs, fetal-**V**CMs, and adult-**V**CMs [10]. Hence, the effect of HDAC inhibition on CMs is also likely to be context-dependent. Indeed, the amount of NPPA mRNA transcripts and the percentage of perinuclear ANF in hESC-**V**CMs are elevated upon VPA treatment. However, since the hESC-**V**CMs are in the early stage of development resembling immature fetal-like heart, where the expression of ANF generally indicates a functional myocardium that is undergoing maturation, the upregulation of ANF in VPA-treated hESC-**V**CMs suggests that HDAC inhibition induces growth and physical maturation. In our present study, hypertrophy was assessed by measurements of capacitance, a physical parameter that directly reflects the cell size based on the membrane lipid bilayer; by contrast, a simple increase in the surface area of cells conventionally grown two-dimensionally may not be due to an increase in size, but other changes such as cellular senescence or flattening. Indeed, hESC-**V**CMs are routinely cultured in monolayer forms, and therefore, it is not possible to assess tissue architecture or hemodynamic load *per se*, reflecting the urgent need of developing three-dimensional experimental for studying these critical properties.

The involvement of chromatin remodeling is shown by immunoprecipitation of H3K4me3, where the level of H3K4me3 is significantly increased on the *ANF* promoter

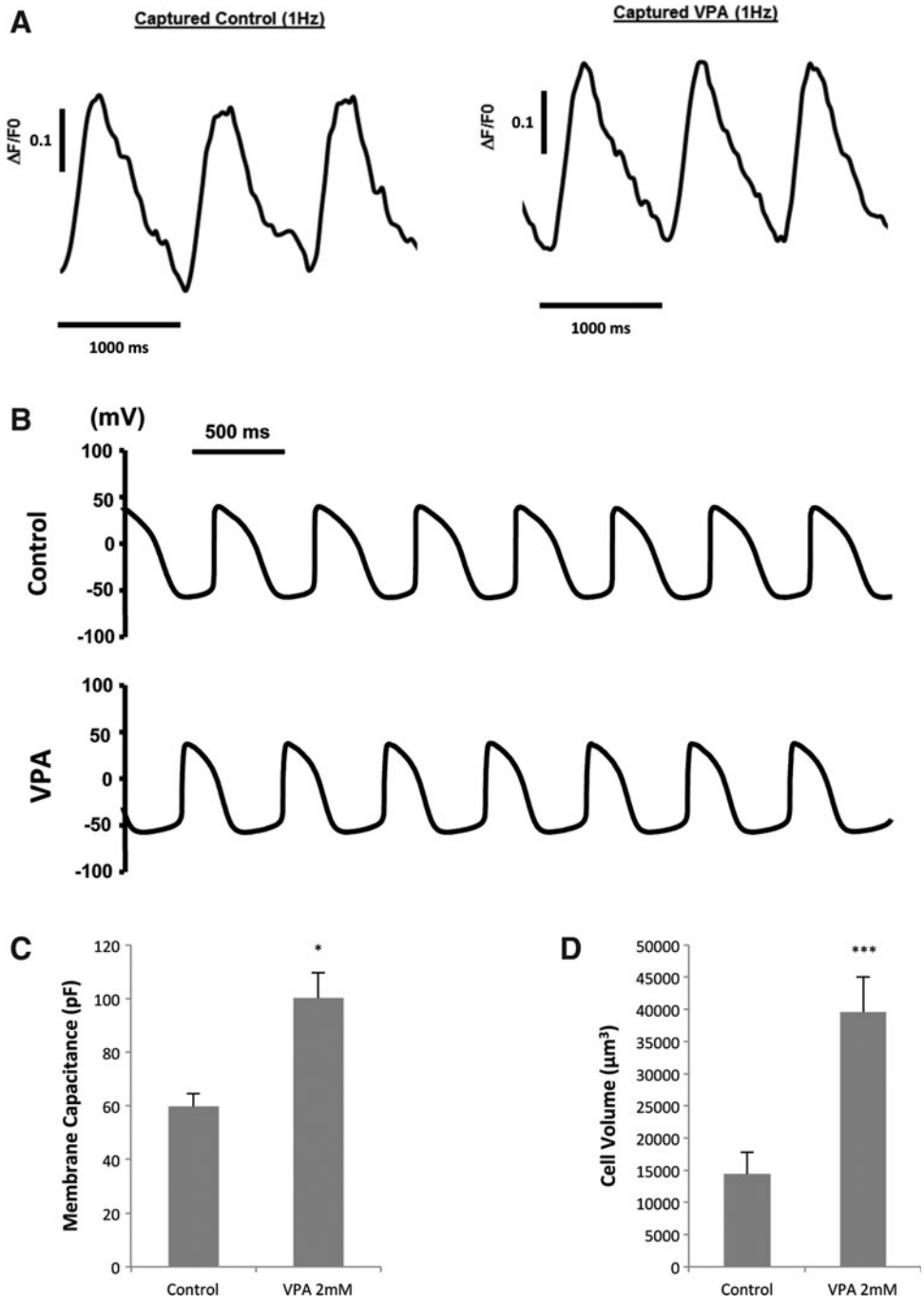

FIG. 6. VPA has no significant effects on the electrophysiological properties of hESC-VCMs. HESC-VCMs were treated with 2 mM of VPA for 72 h and the electrophysiology parameters were measured by calcium imaging and patch clamp. Representative **(A)** Ca^{2+}-transient and **(B)** AP tracings of control and VPA-treated hESC-VCMs. **(C)** Membrane capacitance of control and VPA-treated hESC-VCMs (results from three independent experiments). $^{*}P < 0.05$ (Student's *t*-test). **(D)** The cell volume measured by z-stack image obtained from immunofluorescence imaging. Data shown as mean ± standard deviations. $^{***}P < 0.001$ (Student's *t*-test).

Table 2. Action Potential Analysis (Patch Clamp)

	Control (n = 43)	*VPA (n = 25)*
Amplitude (mV)	84.16 ± 2.97	81.23 ± 2.17
Upstroke velocity (mV/ms)	19.15 ± 2.19	22.88 ± 2.53
Decay velocity (mV/ms)	− 0.42 ± 0.05	− 0.52 ± 0.24
APD50 (ms)	268.85 ± 46.86	233.28 ± 26.13
ADP90 (ms)	351.14 ± 54.05	291.66 ± 27.33
MDP (mV)	− 62.61 ± 1.73	66.04 ± 1.78
Membrane capacitance (pF)	59.77 ± 4.69	100.17 ± 9.24*

$^{*}P < 0.05$.

following exposure to VPA. Furthermore, the VPA treatment shows increased levels of Ca^{2+} handling and cardiac ion channel gene expressions. However, it remains to be determined if this transient inhibition of HDAC could have elicited an epigenetic memory in the CMs as with complications of diabetes, where endothelial cells with prior exposure of hyperglycemia lead to various histone methylation and demethylation events that impact on the gene activity, where proinflammatory pathways are permanently activated [57]. Further understanding of the chromatin remodeling events and how they are linked to cardiac differentiation and maturation will lead to better strategies to pluripotent stem cell-based disease modeling and therapies.

Conclusion

In conclusion, this study describes a dynamic shift of transcription determining histone methylation marks on the promoters of genes associated with pluripotency maintenance, mesodermal and cardiac lineage, Ca^{2+}-handling proteins, and cardiac ion channels in hESCs upon directed CM differentiation. The introduction of transient HDAC inhibition in hESC-**V**CMs amplifies the expression level of specific genes important for CM functions. The fact that discrete histone modifications have been uncovered on both active and silent promoters highlights the importance of the orchestration of epigenetic mechanisms in transcriptional regulation, and therefore, the phenotype of hESC-**V**CMs. We conclude that although hESC-**V**CMs display immature structural and functional properties, their epigenetic state is dynamic and when appropriately activated, display traits consistent with maturation. These findings raise the intriguing possibility of using epigenetic modifiers in combination with other promaturation stimuli such as environmental cues to drive in vitro global maturation of hESC-**V**CMs toward an adult-like phenotype.

Acknowledgment

This work was supported by grants from the Research Grant Council (TBRS T13-706/11 and GRF 103544).

Author Disclosure Statement

No competing financial interests exist.

References

1. Thomson JA, J Itskovitz-Eldor, SS Shapiro, MA Waknitz, JJ Swiergiel, et al. (1998). Embryonic stem cell lines derived from human blastocysts. Science 282:1145–1147.
2. Blin G, D Nury, S Stefanovic, T Neri, O Guillevic, et al. (2010). A purified population of multipotent cardiovascular progenitors derived from primate pluripotent stem cells engrafts in postmyocardial infarcted nonhuman primates. J Clin Invest 120:1125–1139.
3. Blin G, T Neri, S Stefanovic and M Puceat. (2010). Human embryonic and induced pluripotent stem cells in basic and clinical research in cardiology. Curr Stem Cell Res Ther 5:215–226.
4. Yi BA, O Wernet and KR Chien. (2010). Pregenerative medicine: developmental paradigms in the biology of cardiovascular regeneration. J Clin Invest 120:20–28.
5. Laflamme MA, KY Chen, AV Naumova, V Muskheli, JA Fugate, et al. (2007). Cardiomyocytes derived from human embryonic stem cells in pro-survival factors enhance function of infarcted rat hearts. Nat Biotechnol 25:1015–1024.
6. Irion S, MC Nostro, SJ Kattman and GM Keller. (2008). Directed differentiation of pluripotent stem cells: from developmental biology to therapeutic applications. Cold Spring Harb Symp Quant Biol 73:101–110.
7. He JQ, Y Ma, Y Lee, JA Thomson and TJ Kamp. (2003). Human embryonic stem cells develop into multiple types of cardiac myocytes: action potential characterization. Circ Res 93:32–39.
8. Moore JC, J Fu, YC Chan, D Lin, H Tran, et al. (2008). Distinct cardiogenic preferences of two human embryonic stem cell (hESC) lines are imprinted in their proteomes in the pluripotent state. Biochem Biophys Res Commun 372:553–558.
9. Liu J, JD Fu, CW Siu and RA Li. (2007). Functional sarcoplasmic reticulum for calcium handling of human embryonic stem cell-derived cardiomyocytes: insights for driven maturation. Stem Cells 25:3038–3044.
10. Lieu DK, J Liu, CW Siu, GP McNerney, HF Tse, et al. (2009). Absence of transverse tubules contributes to non-uniform Ca(2+) wavefronts in mouse and human embryonic stem cell-derived cardiomyocytes. Stem Cells Dev 18:1493–1500.
11. Poon E, CW Kong and RA Li. (2011). Human pluripotent stem cell-based approaches for myocardial repair: from the electrophysiological perspective. Mol Pharm 8:1495–1504.
12. Klose RJ and Y Zhang. (2007). Regulation of histone methylation by demethylimination and demethylation. Nat Rev Mol Cell Biol 8:307–318.
13. Ruthenburg AJ, H Li, DJ Patel and CD Allis. (2007). Multivalent engagement of chromatin modifications by linked binding modules. Nat Rev Mol Cell Biol 8:983–994.
14. Bannister AJ and T Kouzarides. (2011). Regulation of chromatin by histone modifications. Cell Res 21:381–395.
15. Schneider R, AJ Bannister, FA Myers, AW Thorne, C Crane-Robinson, et al. (2004). Histone H3 lysine 4 methylation patterns in higher eukaryotic genes. Nat Cell Biol 6:73–77.
16. Goldberg AD, CD Allis and E Bernstein. (2007). Epigenetics: a landscape takes shape. Cell 128:635–638.
17. Jenuwein T and CD Allis. (2001). Translating the histone code. Science 293:1074–1080.
18. Rada-Iglesias A and J Wysocka. (2011). Epigenomics of human embryonic stem cells and induced pluripotent stem cells: insights into pluripotency and implications for disease. Genome Med 3:36.
19. Couture JF and RC Trievel. (2006). Histone-modifying enzymes: encrypting an enigmatic epigenetic code. Curr Opin Struct Biol 16:753–760.
20. Campos EI and D Reinberg. (2009). Histones: annotating chromatin. Annu Rev Genet 43:559–599.
21. Schwartz YB and V Pirrotta. (2007). Polycomb silencing mechanisms and the management of genomic programmes. Nat Rev Genet 8:9–22.
22. Barski A, S Cuddapah, K Cui, TY Roh, DE Schones, et al. (2007). High-resolution profiling of histone methylations in the human genome. Cell 129:823–837.
23. Bernstein BE, TS Mikkelsen, X Xie, M Kamal, DJ Huebert, et al. (2006). A bivalent chromatin structure marks key developmental genes in embryonic stem cells. Cell 125:315–326.
24. Mikkelsen TS, M Ku, DB Jaffe, B Issac, E Lieberman, et al. (2007). Genome-wide maps of chromatin state in pluripotent and lineage-committed cells. Nature 448:553–560.
25. Guenther MG, SS Levine, LA Boyer, R Jaenisch and RA Young. (2007). A chromatin landmark and transcription initiation at most promoters in human cells. Cell 130:77–88.
26. Yang L, MH Soonpaa, ED Adler, TK Roepke, SJ Kattman, et al. (2008). Human cardiovascular progenitor cells develop from a KDR+ embryonic-stem-cell-derived population. Nature 453:524–528.
27. Fu JD, P Jiang, S Rushing, J Liu, N Chiamvimonvat, et al. (2010). Na+/Ca2+ exchanger is a determinant of excitation-contraction coupling in human embryonic stem cell-derived ventricular cardiomyocytes. Stem Cells Dev 19:773–782.
28. Fu JD, SN Rushing, DK Lieu, CW Chan, CW Kong, et al. (2011). Distinct roles of microRNA-1 and −499 in ventricular specification and functional maturation of human embryonic stem cell-derived cardiomyocytes. PLoS One 6:e27417.

29. Marks PA, VM Richon, WK Kelly, JH Chiao and T Miller. (2004). Histone deacetylase inhibitors: development as cancer therapy. Novartis Found Symp 259:269–281; discussion 281–288.
30. Wolffe AP and MA Matzke. (1999). Epigenetics: regulation through repression. Science 286:481–486.
31. Cameron EE, KE Bachman, S Myohanen, JG Herman and SB Baylin. (1999). Synergy of demethylation and histone deacetylase inhibition in the re-expression of genes silenced in cancer. Nat Genet 21:103–107.
32. Stein AB, TA Jones, TJ Herron, SR Patel, SM Day, et al. (2011). Loss of H3K4 methylation destabilizes gene expression patterns and physiological functions in adult murine cardiomyocytes. J Clin Invest 121:2641–2650.
33. Liu Z, T Li, Y Liu, Z Jia, Y Li, et al. (2009). WNT signaling promotes Nkx2.5 expression and early cardiomyogenesis via downregulation of Hdac1. Biochim Biophys Acta 1793:300–311.
34. Zhang CL, TA McKinsey, S Chang, CL Antos, JA Hill, et al. (2002). Class II histone deacetylases act as signal-responsive repressors of cardiac hypertrophy. Cell 110:479–488.
35. Wamstad JA, JM Alexander, RM Truty, A Shrikumar, F Li, et al. (2012). Dynamic and coordinated epigenetic regulation of developmental transitions in the cardiac lineage. Cell 151:206–220.
36. Paige SL, S Thomas, CL Stoick-Cooper, H Wang, L Maves, et al. (2012). A temporal chromatin signature in human embryonic stem cells identifies regulators of cardiac development. Cell 151:221–232.
37. Lieu DK, JD Fu, N Chiamvimonvat, KC Tung, GP McNerney, et al. (2013). Mechanism-based facilitated maturation of human pluripotent stem cell-derived cardiomyocytes. Circ Arrhythm Electrophysiol 6:191–201.
38. Kaichi S, K Hasegawa, T Takaya, N Yokoo, T Mima, et al. (2010). Cell line-dependent differentiation of induced pluripotent stem cells into cardiomyocytes in mice. Cardiovasc Res 88:314–323.
39. Kawamura T, K Ono, T Morimoto, H Wada, M Hirai, et al. (2005). Acetylation of GATA-4 is involved in the differentiation of embryonic stem cells into cardiac myocytes. J Biol Chem 280:19682–19688.
40. Johannessen CU and SI Johannessen. (2003). Valproate: past, present, and future. CNS Drug Rev 9:199–216.
41. Bradbury CA, FL Khanim, R Hayden, CM Bunce, DA White, et al. (2005). Histone deacetylases in acute myeloid leukaemia show a distinctive pattern of expression that changes selectively in response to deacetylase inhibitors. Leukemia 19:1751–1759.
42. Harikrishnan KN, TC Karagiannis, MZ Chow and A El-Osta. (2008). Effect of valproic acid on radiation-induced DNA damage in euchromatic and heterochromatic compartments. Cell Cycle 7:468–476.
43. Binah O, K Dolnikov, O Sadan, M Shilkrut, N Zeevi-Levin, et al. (2007). Functional and developmental properties of human embryonic stem cells-derived cardiomyocytes. J Electrocardiol 40:S192–S196.
44. Liu J, DK Lieu, CW Siu, JD Fu, HF Tse, et al. (2009). Facilitated maturation of Ca2+ handling properties of human embryonic stem cell-derived cardiomyocytes by calsequestrin expression. Am J Physiol Cell Physiol 297: C152–C159.
45. Lieu DK, YC Chan, CP Lau, HF Tse, CW Siu, et al. (2008). Overexpression of HCN-encoded pacemaker current silences bioartificial pacemakers. Heart Rhythm 5:1310–1317.
46. Chan YC, CW Siu, YM Lau, CP Lau, RA Li, et al. (2009). Synergistic effects of inward rectifier (I) and pacemaker (I) currents on the induction of bioengineered cardiac automaticity. J Cardiovasc Electrophysiol 20:1048–1054.
47. Backs J, K Song, S Bezprozvannaya, S Chang and EN Olson. (2006). CaM kinase II selectively signals to histone deacetylase 4 during cardiomyocyte hypertrophy. J Clin Invest 116: 1853–1864.
48. Bush E, J Fielitz, L Melvin, M Martinez-Arnold, TA McKinsey, et al. (2004). A small molecular activator of cardiac hypertrophy uncovered in a chemical screen for modifiers of the calcineurin signaling pathway. Proc Natl Acad Sci U S A 101:2870–2875.
49. Chang S, TA McKinsey, CL Zhang, JA Richardson, JA Hill, et al. (2004). Histone deacetylases 5 and 9 govern responsiveness of the heart to a subset of stress signals and play redundant roles in heart development. Mol Cell Biol 24:8467–8476.
50. Bradner JE, N West, ML Grachan, EF Greenberg, SJ Haggarty, et al. (2010). Chemical phylogenetics of histone deacetylases. Nat Chem Biol 6:238–243.
51. Antos CL, TA McKinsey, M Dreitz, LM Hollingsworth, CL Zhang, et al. (2003). Dose-dependent blockade to cardiomyocyte hypertrophy by histone deacetylase inhibitors. J Biol Chem 278:28930–28937.
52. Cardinale JP, S Sriramula, R Pariaut, A Guggilam, N Mariappan, et al. (2010). HDAC inhibition attenuates inflammatory, hypertrophic, and hypertensive responses in spontaneously hypertensive rats. Hypertension 56:437–444.
53. Cao DJ, ZV Wang, PK Battiprolu, N Jiang, CR Morales, et al. (2011). Histone deacetylase (HDAC) inhibitors attenuate cardiac hypertrophy by suppressing autophagy. Proc Natl Acad Sci U S A 108:4123–4128.
54. Kong Y, P Tannous, G Lu, K Berenji, BA Rothermel, et al. (2006). Suppression of class I and II histone deacetylases blunts pressure-overload cardiac hypertrophy. Circulation 113:2579–2588.
55. Ahmad F, JG Seidman and CE Seidman. (2005). The genetic basis for cardiac remodeling. Annu Rev Genomics Hum Genet 6:185–216.
56. Moorman AF and VM Christoffels. (2003). Cardiac chamber formation: development, genes, and evolution. Physiol Rev 83:1223–1267.
57. Brasacchio D, J Okabe, C Tikellis, A Balcerczyk, P George, et al. (2009). Hyperglycemia induces a dynamic cooperativity of histone methylase and demethylase enzymes associated with gene-activating epigenetic marks that coexist on the lysine tail. Diabetes 58:1229–1236.

Address correspondence to:
Prof. Ronald Li
Stem Cell and Regenerative Medicine Consortium (SCRMC)
The University of Hong Kong
Hong Kong Jockey Club Building
for Interdisciplinary Research
5 Sassoon Road
Pok Fu Lam
Hong Kong

E-mail: ronaldli@hkucc.hku.hk; ronald.li@mssm.edu

Received for publication March 6, 2013
Accepted after revision May 8, 2013
Prepublished on Liebert Instant Online May 8, 2013